Contrib. Plasma Phys. **45**, No. 5-6, 369 – 377 (2005) / **DOI** 10.1002/ctpp.200510042

Analysis and Kinetics of Transient Species in Electrode Near Plasma and Plasma Boundary Sheath of RF Plasmas in Molecular Gases

M. Geigl, S. Peters[*]**, O. Gabriel, B. Krames,** and **J. Meichsner**[**]

Ernst Moritz Arndt University Greifswald, Institute of Physics, Domstr. 10a, D-17489 Greifswald

Received 09 May 2005, accepted 13 June 2005
Published online 29 July 2005

Key words Rf plasma, fluorocarbon plasma, oxygen plasma, two-photon absorption laser induced fluorrecence spectroscopy, time resolved threshold ionization mass spectrometry, similarity parameter, radical kinetics.
PACS 42.62.Fi, 52.27.Cm, 52.80.Pi, 82.80.Ms

Modern diagnostic methods are applied for investigation of spatial and temporal behaviour of selected reactive species in oxygen and fluorocarbon rf plasmas. Comprehensive investigations of the spatial distribution of atomic oxygen were done by means of two-photon absorption laser induced fluorescence spectroscopy. Exemplarily, axial and radial O-concentrations are shown for an asymmetric capacitively coupled rf plasma in pure oxygen. The time resolved threshold ionization mass spectrometry was applied for investigation of small fluorocarbon radicals. In pulsed CF_4/H_2 rf plasma the concentrations of the extracted radicals CF_2, CF_3, C_2F_5 as well as the intermediate product C_2F_4 in the plasma on and off phase are presented.

© 2005 WILEY-VCH Verlag GmbH & Co. KGaA, Weinheim

1 Introduction

Knowledge of concentration and kinetics of transient reactive species in molecular low pressure plasmas are of great interest because of their important role in plasma chemical gas conversion and reactive plasma surface interaction. In particular, the highly reactive species such as atomic oxygen or fluorine are the important reaction partners in surface oxidation/fluorination, modification of polymers or plasma etching [1, 2]. On the other hand, small fluorocarbon radicals, such as CF, CF_2, CF_3, are important species for formation of compounds with higher molecular weight (oligomers) and precursors in thin film deposition [3, 4]. In particular, the fluorocarbon species which are immediately involved in the thin film growth are not clearly defined. Furthermore, the thin film formation represents a complex process which includes plasma etching and deposition simultaneously. From the experimental point of view the spatio-temporal behaviour and quantitative analysis of reactive neutral species concentrations are in the focus of this paper. Nevertheless, diagnostic methods are restricted for specific kind of species or limited in time and space resolution due to their applied physical/chemical principle of detection.

In this paper two experimental methods were applied, the

(i) Two-photon absorption laser induced fluorescence (TALIF), and the
(ii) Threshold ionization mass spectrometry (TMS).

Both methods have been applied successfully in other experimental works [5–11]. Here, the study of atomic oxygen by means of TALIF were done with the aim to describe the atomic oxygen distribution by similarity parameters which include total pressure, discharge geometry and discharge parameters (e.g. self bias voltage) of a capacitively coupled oxygen rf plasma. Therefore, comprehensive investigations were done to analyse the spatial and temporal behaviour of atomic oxygen in the complete discharge zone including the plasma sheath. In this paper, some selected results are presented from continuous discharge mode.

[*] Present address: Institute of Low Temperature Plasma Physics, Friedrich-Ludwig-Jahn-Str. 19, 17489 Greifswald, Germany
[**] Corresponding author: e-mail: meichsner@physik.uni-greifswald.de

© 2005 WILEY-VCH Verlag GmbH & Co. KGaA, Weinheim

The TMS was applied for the time resolved analysis of small fluorocarbon radicals. The neutral transient species from pulsed CF_4/H_2 rf plasma were directly extracted into a two stage pumped mass spectrometer system. At known electron impact ionization cross sections of the involved species and the calibration of the mass spectrometer, the kinetics of CF_2, CF_3, C_2F_5 radicals and C_2F_4 as a stable intermediate reaction product could be studied.

2 Experimental setup and Methods

2.1 Oxygen plasma and two photon absorption laser induced fluorescence (TALIF)

The low pressure plasma was performed in pure oxygen by capacitive excitation at a radio frequency (rf) of 13.56 MHz. The parallel plate discharge configuration consisted of two circular stainless steel electrodes, 80 mm in diameter, with horizontal orientation. Both of them were covered by a grounded shield and the electrode gap d was variable from 25 mm up to 100 mm. The rf power was generated by an ENI power supply connected to the driven (rf) electrode via matching network unit (ENI). The other one was connected to ground potential. The asymmetric coupling leads to a self bias voltage of -100 V up to -500 V, depending on the discharge power, which was in the range of 20 W up to 140 W.

The pump assembly consisted of a turbo-molecular pump and rotary vane pump (ILMVAC) for reactive gases. Without any working gas an ultimate pressure of 10^{-6} Pa was reached. A MKS mass flow controller provided a constant oxygen gas flow of 3 sccm, and the pressure was controlled by a downstream throttle valve combined with a control unit (MKS). In experiments the discharge pressure was varied from 10 Pa to 100 Pa.

A well established technique to measure atomic oxygen concentration is the two-photon absorption laser induced fluorescence (TALIF), which has been successfully applied in several experimental works, [5–8]. The chosen transition $3p^3P_{2,1,0} \rightarrow 2p^3P_2$ was utilized to excite the atomic species from the ground state by absorption of two photons at λ = 225.6 nm. Once excited to this state, the O-atom fluoresces back to the $3s^3S_1^0$ state and the emission was detected at λ = 844.6 nm. Absolute atomic oxygen concentrations are estimated by calibration with neutral xenon gas. The reference measurement with xenon gas of known density is applied due to two-photon resonance $5p^6\,{}^1S_0 \rightarrow 5p^5 7p[3/2]_2$ at λ = 225.4nm [12–14], which is spectrally close to the oxygen resonance. In this case more than one fluorescence channels exist: $7p[3/2]_2 \rightarrow 7s, 6s, 6s'$.

Tuneable radiation in the 226 nm region was produced by frequency doubling the laser light of the dye laser system (LAS). The third harmonic of the Nd:YAG laser (Quanta Ray, 10 Hz, pulse duration 8 ns) pumped a 1:1 admixture of Coumarin 47 and Coumarin 120 at λ = 452 nm. Passing through a non linear crystal (BBO-I), the desired UV radiation with a pulse energy in the range of 350μJ was generated and separated by a Pellin Broca prism. The beam focused by a quartz lens (f = 300 mm) crossed the discharge cell parallel to the electrodes. A power meter (LAS) measured the laser energy per shot. Perpendicular to the laser beam the fluorescence light was collected by a focusing lens (f = 175 mm) and directed through a 10 nm FWHM interference filter centred at 846 nm on a photomultiplier tube (PMT, Hamamatsu). The PMT signal was given to a boxcar, where it was averaged over 50 - 250 laser shots, depending on the signal to noise ratio.

The optical setup required for calibration was the same. After turning off the discharge the vacuum vessel was filled with pure xenon gas. Pressures up to 5 Pa assured a suitable small self-quenching rate and the fluorescence line $7p \rightarrow 6s$ (λ = 462 nm) was singled out by a second interference filter (FWHM 10 nm). Due to the fine structure of the atomic ground state levels, the O atom temperature was determined by Boltzmann distribution, while the xenon temperature was estimated to 300 K. A sketch of the experimental setup is shown in Fig. 1.

For spatial resolved measurements the electrode system was mounted on an axial/radial-translation stage and moved with respect to the fixed optical arrangement inside the vacuum vessel (300 mm in diameter). Thus, the discharge region could be monitored between the electrode gap (axial direction) and along the electrode diameter (radial direction), see Fig. 1. In principal, the laser spot size limited the spatial resolution. It was estimated to 0.1 mm. Therefore, a minimum step of 0.5 mm was chosen for axial measurements and positions close to the electrode surfaces. In radial direction, the spatial resolution of the manipulation system confines the step width to 1.5 mm.

© 2005 WILEY-VCH Verlag GmbH & Co. KGaA, Weinheim

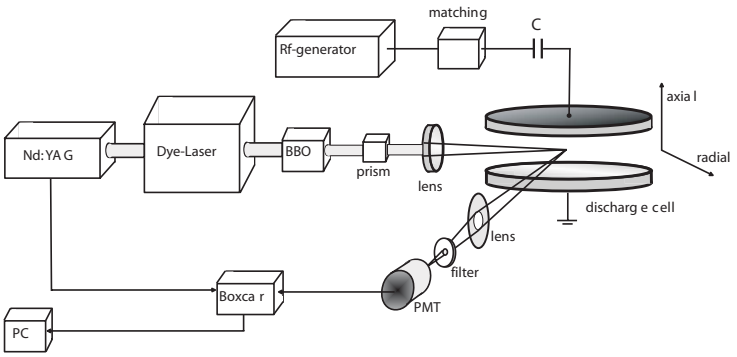

Fig. 1 Optical arrangement for spatially resolved two photon laser induced fluorescence spectroscopy.

2.2 Fluorocarbon plasmas and time resolved threshold ionization mass spectrometry (TMS)

The apparatus for mass spectrometric investigations is similar to the TALIF experiment. It consists of a stainless steel vacuum chamber, vacuum equipment and parallel plate discharge electrodes with a diameter of 80 mm and a gap of 40 mm. A low pressure capacitively coupled rf plasma at 13.56 MHz was generated in a mixture of tetrafluoromethan (CF_4) and hydrogen (H_2). Transient fluorocarbon species of the rf plasma were extracted into a two stage pumped quadruple mass spectrometer (HIDEN EQP 1000). The aperture (diameter 400 μm) of the mass spectrometer was inserted into the grounded electrode, see Fig. 2.

In contrast to the pure oxygen discharge with one neutral radical (atomic oxygen), the fluorocarbon plasma is characterized by a mixture of small fluorocarbon radicals e.g. CF, CF_2, CF_3 from CF_4 dissociation, and additional reaction products, e.g. C_2F_4, C_2F_5, C_2F_6, C_3F_7, C_3F_8.

The threshold ionization mass spectrometry was applied to analyse such neutral transient fluorocarbon species from CF_4/H_2-plasmas. At the given geometry and efficiency of turbo-molecular pumps the optimal conditions for collision-less extraction of transient species could be realized for total pressure lower than 50 Pa. In the ion source of the mass spectrometer the extracted neutrals were ionized due to the crossing of the molecular beam of extracted species with an electron beam at chosen electron energy. Depending on the ionization threshold the detected positive ion (e.g. CF_3^+) have their origin from different molecules (e.g. CF_3, CF_4) by direct or dissociative ionization. Tuning the electron energy in the region of the threshold energy (typically 10-25 eV) the extracted neutral radicals could be separated from the total ion signal if the partial ionization cross sections were known, see Fig. 3.

Above the threshold energies the ion signal consists of the sum of contributions from different neutrals. The measured ion signal (S_i) depends on the number density of neutrals (n_M), the corresponding ionization cross section (σ), the electron current in the ion source (I_e) and the apparatus function (α) which includes geometry, ion transmission in quadruple and detector sensitivity [15].

$$S_i = \sum_M n_M \cdot \sigma(M \rightarrow i^+) \cdot I_e \cdot \alpha \tag{1}$$

In the case of known electron impact cross sections the number densities of neutrals were estimated by a least-square-fitting procedure on the measured ion signal. Here, it was applied a fit procedure "lfit" from "Numerical Recipes in C" [16] which was modified in X_k.

$$y(x) = \sum_{k=1}^{N} a_k \cdot X_k(x) \qquad \text{with} \qquad a_k = n_k \cdot I_e \cdot \alpha_k \tag{2}$$

The term $X_k(x)$ contains the used cross sections from experiments or theoretical calculations with specific approximations. Therefore, the error of cross sections has to be taken into calculation by use of formular (3). Due to an iteration procedure the function χ^2 was minimised until the changes were lower than 10^{-5}.

© 2005 WILEY-VCH Verlag GmbH & Co. KGaA, Weinheim

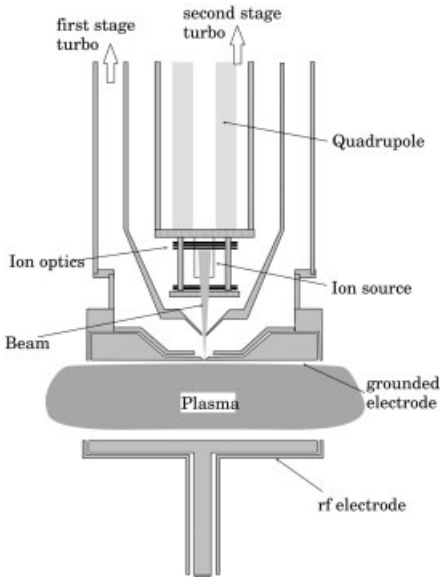

Fig. 2 Profile of the two stage pumped quadruple mass spectrometer and arrangement for extraction of transient neutral species from rf plasma.

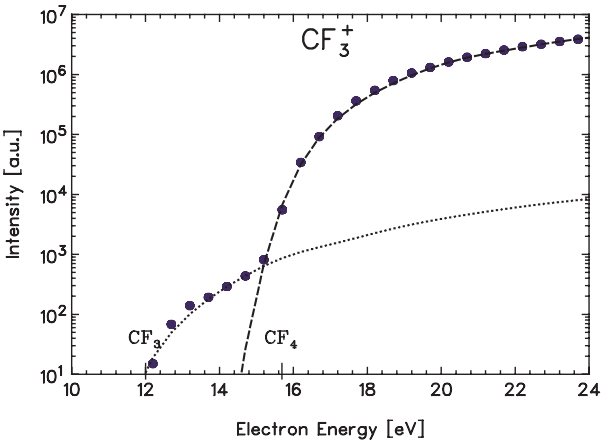

Fig. 3 Example for detection of CF_3 radicals by threshold ionization mass spectrometry (dots: measurement, lines: fitted curves by use of the electron impact cross section for generation of CF_3^+ ions from CF_3 and CF_4.

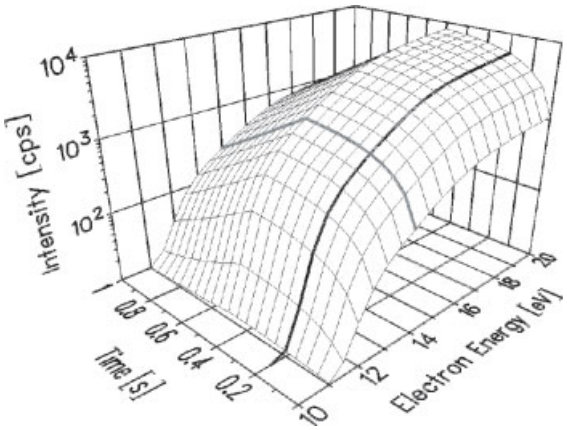

Fig. 4 Principle of time resolved threshold ionization mass spectrometry. For selected time slot of a pulsed plasma the signal intensity is measured for chosen positive fragment ion in dependence on electron energy.

$$\chi^2 = \sum_{i=1}^{N} \frac{(y_i - \sum_k a_k \cdot X(x_i))^2}{\sigma_{yi}^2 + \sum_k a_k^2 \cdot \sigma_{xk}^2} \tag{3}$$

The electron energy in the ion source was calibrated by use of argon as reference gas with a well known threshold energy at 15.76 eV. Additionally, a Gaussian energy distribution of the electrons in the ion source with ΔE = 0.9 eV (FWHM) was included in the calculation. The apparatus function was estimated for stable species with known concentration, and it was applied for calculation of absolute radical concentrations.

For time resolved radical analysis the mass spectrometer was combined with a multi-channel scaler (MCS-pci, ORTEC Co.). The time resolution was limited by the ion transmission time inside the mass spectrometer system (aperture - detector), which was in the order of some 10μs. The MCS allows to set a number of time slots for selected detection of ion signals directly from the channeltron ion detector (TTL-signals) of the mass spectrometer.

Synchronisation between the pulsed plasma and the multi-channel scaler by means of a pulse delay generator allowed time resolved measurements of radical concentrations. For example, the pulsed rf plasma of 1 Hz pulse

© 2005 WILEY-VCH Verlag GmbH & Co. KGaA, Weinheim

frequency and 0.5 duty cycle needs 10^3 time slots for time resolution of 1ms. Signal accumulation over 100 pulses provided a total integration time of 100 ms per time slot which was mostly sufficient to receive appropriate signal to noise ratio. For a given number of time slots within the pulse period the time depending ion signal was measured for fixed electron energy. By scanning the electron energy step by step, typically 0.5 eV, the time and energy resolved ion signal could be reconstructed, see Fig. 4.

3 Results and Discussion

3.1 Atomic oxygen distribution in pure oxygen rf plasmas

Depending on the plasma parameters and the electrode distance the spatial density structure of the atomic oxygen was measured in two dimensions, axial and radial. Absolute values were obtained in the middle of the discharge. Here the O atom temperature was in the range of 450 K, because of the non-cooled electrode system. This was in accordance with the temperature range found by Gomez et al. [7] in a capacitive mode of an inductively coupled oxygen rf plasma.

For a typical self bias voltage of U_b = - 320 V absolute densities were determined to 0.8 - 4.4 10^{13} cm^{-3} at a pressure range of 30 - 100 Pa, which was in good agreement with results of Goehlich et al. [13], measured under comparable discharge conditions.

Axial density distribution

Axial density distributions are exemplarily shown for two different total pressures in Fig. 5. Inside the quasi-neutral plasma the atomic oxygen density was almost constant. Diffusion and surface recombination represent the prominent loss processes of the atomic species. Therefore, in front of the electrodes the density gradients were found due to different loss rates. A strong decrease of O-density can be seen in the region near to the rf electrode, while a smoother one appeared close to the grounded electrode. At smaller electrode gap d, in the range of 25 mm, the density profiles exhibited a more round, nearly symmetric shape. In that case the loss of O atoms is dominated by surface recombination which determines the spatial distributions. Comparable behaviour can be found at Tserepi et al. [8], using an electrode separation of 18 mm in their experiments. At larger gap width the curves flattened in the plasma centre and the profiles showed an asymmetric shape. To analyze qualitatively the atomic oxygen flux to the electrode surfaces, the profiles were normalized to an averaged O-density in the middle of the discharge. Likewise the shadowing of the fluorescence signal near to the electrodes was corrected by factors acquired by TALIF measurements in pure xenon.

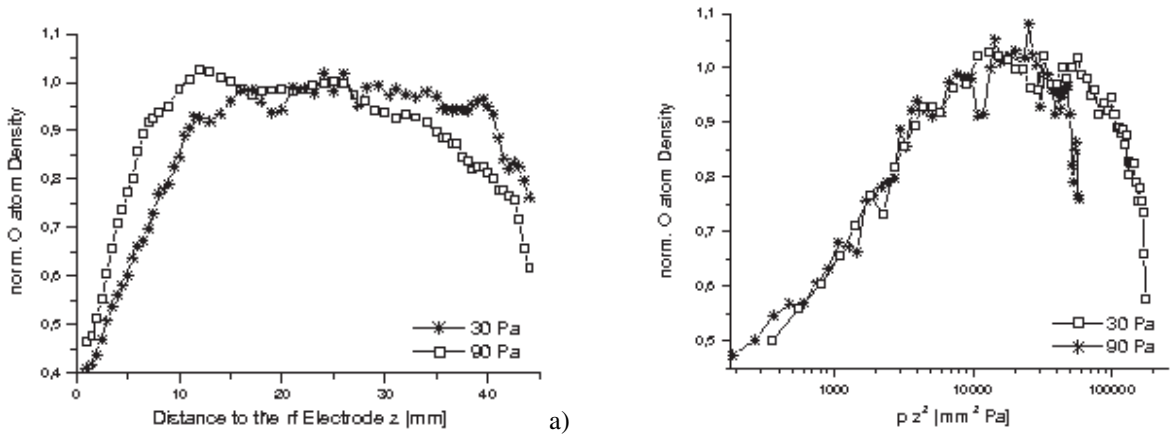

Fig. 5 (a) Asymmetric axial O density distributions (normalized to the discharge centre) represent the asymmetric capacitively coupled plasma with different sheath properties in front of the driven and grounded electrode. (b) The behaviour in front of the rf electrode (rf sheath) can be described by an empiric similarity parameter $p \times z^2$ (z: distance to the rf electrode), self-bias voltage U_b = -377 V, electrode gap d = 45 mm).

This is mainly a result of the change of the rf plasma and rf sheath properties at the driven electrode and the diffusion controlled transport of atomic oxygen due to their long collision lifetime. Close to the driven electrode

© 2005 WILEY-VCH Verlag GmbH & Co. KGaA, Weinheim

the profiles are characterized by a strong decrease in direction of the electrode surface. As seen in Fig. 5a, the shape of the axial density distributions is influenced by the total pressure. Due to the smaller thickness of the rf sheath at higher pressure and the reduced diffusion coefficient, the O concentration gradient increases in comparison with lower pressure. Mutsukura et al. [17] described a relationship between the pressure p and the sheath thickness d_s in rf discharges by $p^k \cdot d_s$ = const. In the case of an oxygen plasma k was obtained between 1/3 and 1/4. Assuming the main area of O_2 dissociation by electron impact, which is the significant production mechanism for the ground-state O atoms [18], at the edge of rf sheath the gradient shape has to be related to the rising sheath thickness at decreasing pressure. An analogue expression to the O density in front of the rf electrode was found: an empiric similarity parameter $p \cdot z^2$, (z: distance to the rf electrode). Plotting the normalized curves at different pressures against this relation the shapes became equal, see Fig. 5b. For that consideration a constant self bias voltage U_b was essentially required. Investigations on other plasma species which transport is controlled by diffusion, e.g. ambipolar diffusion of charged particles as well as meta-stable excited species (e.g. nitrogen molecules [19]), revealed the $p \cdot z^2$ dependence of the axial profiles very well. Otherwise a comparative behaviour for the region nearby the grounded electrode could not be applied, whereby the distance to the grounded electrode was taken into consideration.

For increasing electrode gap d the spatial profiles expanded as whole, scaling with the gap for p = constant and U_b =constant. Under the present discharge conditions an upper limit was found for an aspect ratio in the order of one, that means for d = 80 mm. Likewise at lower gap width as investigated, a downward limit had to be expected, too. Due to the confinement of the region of constant O density (described above), it can be imagined that at electrode separations less than 25 mm only the two density gradients are left, shifting into one another. In that case the scaling might be invalid, too.

Radial density distribution

For different axial positions z the radial profiles of the O atom density were studied. Measurements along the whole electrode axis and in the spatial afterglow of the plasma yielded symmetric shapes with respect to the discharge axis (r = 0 mm). Fig. 6a pictured three different curves depending on z at an electrode space of 45 mm. To compare among one another the radial distributions were normalized to the axial density in the discharge centre. In the middle of the discharge, where the axial density was nearly constant (z = 21 mm), the oxygen flux is determined by diffusion from the centre towards the surrounding reactor volume. Therefore the curves show a continuously decreasing density in radial direction. In the case of the grounded electrode this structure is axially

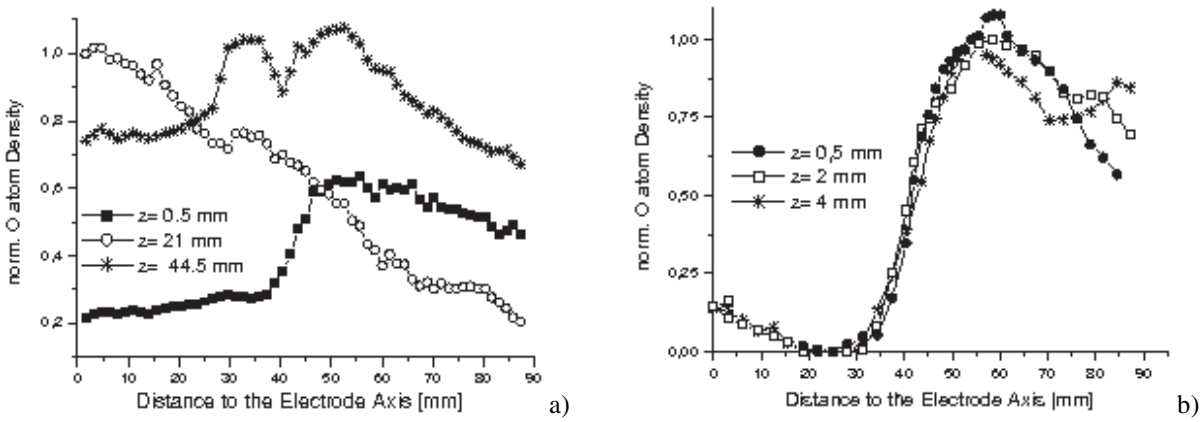

Fig. 6 Density distribution of atomic oxygen in dependence on the radial distance r to the electrode axis: a) Density (normalized to the discharge centre) in front of the driven electrode (z=0.5 mm), in the discharge centre (z=21 mm) and in front of the grounded electrode (z=44.5 mm), and b) Density (normalized to the difference between values at local maximum and minimum near the electrode edge) in front of the driven electrode. (p = 40 Pa, self bias voltage U_b = - 350 V, electrode gap d = 45 mm).

limited in the range of 1-2 mm in front of the electrode surface. Due to the smoother axial concentration decrease, a lower particle loss can be assumed in comparison with the situation in front of the rf electrode. Therefore the

© 2005 WILEY-VCH Verlag GmbH & Co. KGaA, Weinheim

number density increased at shorter distances to the discharge axis and exhibited a wider maximum. The electrode surface acts as a significant sink for O atoms. Comparing radial position in respect to the electrode radius the stronger density decrease is observed for $r < R$. This phenomenon is the result of significant loss processes compared with radial distances outside the electrode edge. Close to both electrodes the number density increased out off the discharge centre and reached a local maximum in the spatial afterglow of the discharge near the electrode edge (r = 40 mm). This suggested an annular shaped plasma around the electrode edge. Similar behaviour was found for other neutral species like ArI in a GEC cell [20] and CF_2 molecules in a CF_4/O_2 rf plasma [21]. The local maximum became less pronounced at larger displacements to the electrodes and disappeared in region where the O atom density is axially constant. Thus, it can be mentioned that surface recombination of the atomic oxygen defines the depth of the observed profiles. In order to proof this presumption the radial distributions were normalized to their radial maximum at different axial positions. For both electrodes the radial shapes were found independent of the axial position under identical plasma condition, see Fig. 6b.

3.2 Small fluorocarbon radicals in CF_4/H_2 rf plasmas

For a pulsed CF_4/H_2-plasma (frequency 1 Hz, duty cycle 0.5) at total pressure of 30 Pa the estimated absolute number densities of CF_2, CF_3, C_2F_4 and C_2F_5 are shown in Fig. 7.

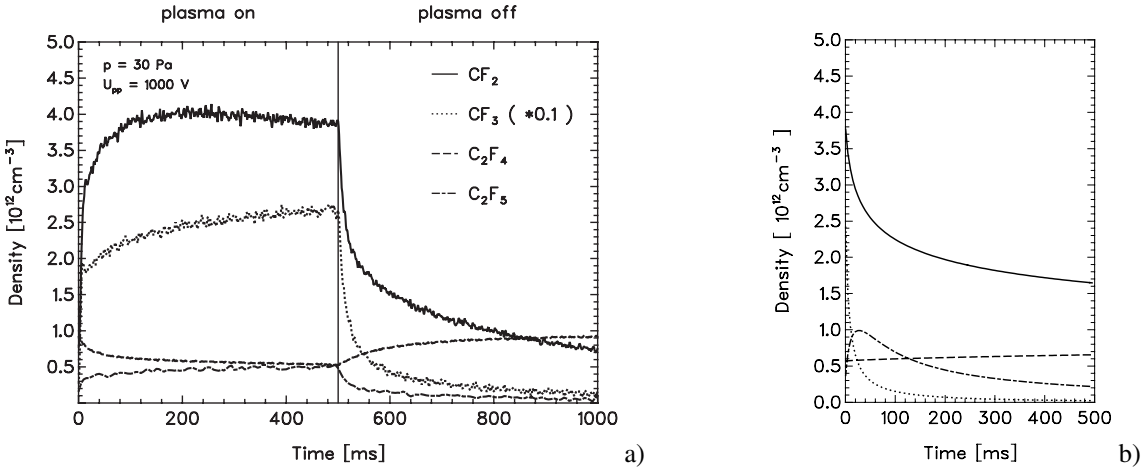

Fig. 7 a) Kinetics of transient species CF_2, CF_3, C_2F_5 and stable reaction product C_2F_4 in a pulsed CF_4/H_2-plasma measured by means of threshold ionization mass spectrometry (13.56 MHz, U_{pp}=1000V, pulse frequency 1 Hz, duty cycle 0.5, 30Pa, CF_4:H_2 3:1, 1.33 sccm). b) The calculated densities of CF_2, CF_3, C_2F_4 and C_2F_5 in the plasma off phase from the rate equation model. The input parameters of the model are the initial densities from the experiment and the rate coefficients from literature, see Table 1.

Reaction					k $(10^{-12}\,\mathrm{cm^3\,s^{-1}})$
CF_2	+	CF_2	$\rightarrow$	C_2F_4	0.04
CF_2	+	CF_3	$\rightarrow$	C_2F_5	1.0
CF_2	+	C_2F_4	$\rightarrow$	C_3F_7	<0.001
CF_2	+	C_2F_5	$\rightarrow$	C_3F_7	0.19
CF_3	+	CF_3	$\rightarrow$	C_2F_6	5.25
CF_3	+	C_2F_4	$\rightarrow$	C_3F_7	$5.4 \cdot 10^{-4}$
C_2F_5	+	C_2F_5	$\rightarrow$	C_4F_{10}	7.0

Table 1 Reactions which are included in the model. Rate constants k were taken from [23].

At the beginning of the plasma pulse the strong increasing CF_2 and CF_3 concentration have their origin in the dissociation of CF_4. Furthermore the free fluorine reacts quickly with hydrogen and forms HF. In result the dominant reaction of fluorine with fluorocarbon radicals back to CF_4 is intermitted. In the plasma off phase the kinetics is determined by heavy particle reactions between fluorocarbon radicals, such as CF, CF_2, CF_3, C_2F_5.

© 2005 WILEY-VCH Verlag GmbH & Co. KGaA, Weinheim

A simple model based on particle balance equations was applied to explain qualitatively the behaviour of CF_2, CF_3 and C_2F_4. The reactions included in this model and their rate constants are shown in Table 1. Note, that the simple model does not include diffusion to the walls and surface reactions. For example, the sticking coefficient of CF_2 on a fluorocarbon film without ion bombardement and UV radiation is in the order of 10^{-5} [22]. Therefore the wall loss was neglected. The fast decrease of the CF_2- and CF_3-density at the beginning of the afterglow and particularly the increase of the C_2F_4-density in the afterglow is reproduced in the model.

A verification of the CF_2 and C_2F_4 kinetics was realized by the IR tuneable diode laser absorption spectroscopy (IR-TDLAS, [24]) at similar experimental conditions. The temporal behaviour of the line integrated CF_2 and C_2F_4 concentrations shows similar behaviour with characteristic formation of the intermediate reaction product C_2F_4 and decreasing CF_2 concentration in the plasma off phase and vice versa in the plasma on phase, see Fig. 8.

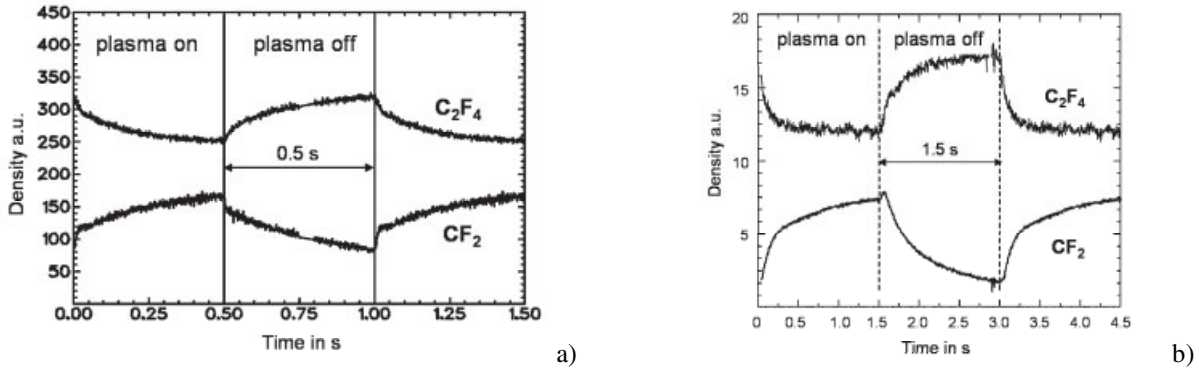

Fig. 8 CF_4/H_2-plasma. CF_2 and C_2F_4 kinetics measured by particle extraction at the grounded electrode with threshold ionization mass spectrometry (left: CF_4:H_2 3:1, 1.33 sccm, 10 Pa, U_{pp}=1000 V, 1 Hz) and by line integrated infrared tuneable diode laser absorption spectroscopy (right: CF_4:H_2 3:1, 13.3 sccm, 20 Pa, 100W, 0.33 Hz).

4 Summary and Conclusions

In this paper the experimental setup and the applied methods of the two-photon absorption laser induced fluorescence (TALIF) and the time resolved threshold ionization mass spectrometry (TMS) were applied for analysis of transient neutral species, such as atomic oxygen and small fluorocarbon radicals.

Selected experimental results are shown and discussed concerning the spatial density distribution of atomic oxygen in pure oxygen rf plasma, and the temporal behaviour of small fluorocarbon radicals in pulsed CF_4/H_2 rf plasmas.

Further considerations involve parameter studies to compare atomic oxygen distribution in capacitively coupled oxygen plasmas by similarity parameters in continuous and pulsed discharge mode. The modelling of the fluorocarbon radical kinetics in pulsed CF_4/H_2 plasmas will be extended by inclusion of additional species and the plasma surface interaction. From the experimental point of view comprehensive studies of fluorocarbon radical densities by use of IR-TDLAS are in progress.

References

[1] T.E.F.M. Standaert, M. Schaepkens et al., J. Vac. Sci. Technol. A **16** (1), (1998).
[2] L. Ling, X. Hua et al., J. Vac. Sci. Technol. A **22** (2), (2004).
[3] J.A. Theil, J. Vac. Sci. Technol. B **17** (6), (1999).
[4] T.E.F.M. Standaert, C. Hedl, et al., J. Vac. Sci. A **22** (1), (2004).
[5] J. Baggermann, R. Visser, E. Collart, J. Appl. Phys.**75** (2), 758 (1994).
[6] D. Bamford, L. Jusinski, W. Bischel, Phys. Rev. E **34** (1), 185 (1986).
[7] S. Gomez, P. Steen, G. Graham, Appl. Phys. Lett. **81**, 19 (2002).
[8] A. Tserepi, T. Miller, J. Appl. Phys. **77**, 505 (1995).
[9] P. Kae-Nune, J. Perrin, J. Guillon, J. Jolly, Plasma Sources Sci. Technol. **4**, 250 (1995).

© 2005 WILEY-VCH Verlag GmbH & Co. KGaA, Weinheim

[10] H. Sugai, H. Toyoda, J. Vac. Sci. Technol. A **10** (4), 1193 (1992).
[11] A.D. Tserepi, W. Schwarzenbach, J. Derouard, N. Sadeghi, J. Vac. Sci. Technol. A **15** (6), 3120 (1997).
[12] L. Cherigier, U. Czarnetzki, D. Luggenhölscher, V. Schulz-von der Gathen, J. Appl. Phys. **85** (2), 696 (1999).
[13] A. Goehlich, T. Kawetzki, H. Döbele, J. Chem. Phys. **108**, 9362 (1998).
[14] K. Niemi, V.S. van der Gathen, H. Döbele, J. Phys. D: Appl. Phys. **34**, 2330 (2001).
[15] H. Singh, J. W. Coburn, D. B. Graves, J. Vac. Sci. Technol. A **17** (5), (1999).
[16] W.H. Press, S.A. Teukolsky, W.T. Vetterling, B.P. Flannery, Numerical recipes in C: the art of scientific computing, 15.4. Cambridge University Press, 2. Ausg. (2002).
[17] N. Mutsukura, K. Kobayashi, Y. Machi, J. Appl. Phys. **68** (6), 2657 (1995).
[18] E.J.H. Collart, J. Visser, J.A.G. Baggermann, J. Appl. Phys. **78** (7), 47 (1995).
[19] B. Krames, Räumliche Konzentrationsverteilungen von N_2-Triplett-Zuständen im elektrodennahen Plasma einer Rf-Niederdruckentladung, Ph.D. thesis, TU Chemnitz, Germany, (2000);
B. Krames, T. Glenewinkel-Meyer, J. Meichsner, J. Phys. D: Appl. Phys. **34**, 1789-1798 (2001).
[20] C. Collard, S. Shannon, J.P. Holloway, M.L. Brake, IEEE Transactions on Plasma Science **28** (6), 2187 (2000).
[21] K.L. Steffens, M.A. Sobolewski, J. Va, Sci. Technol. A **17** (2), 517 (1999).
[22] B.A. Cruden, K. K. Gleason, H.H. Sawin, J. Vac. Sci. Technol. B **20** (2), 690 (2002).
[23] NIST Chemistry WebBook, NIST Standard Reference Database Number 69, http://webbook.nist.gov/chemistry
[24] O. Gabriel, K. Li, J. Meichsner; Conference Proceedings, P. 229-230, ESCAMPIG 17, Constanta, Romania, 1 - 5 September 2004

© 2005 WILEY-VCH Verlag GmbH & Co. KGaA, Weinheim